IEEE Access
Multidisciplinary | Rapid Review | Open Access Journal

Received 4 January 2024, accepted 29 January 2024, date of publication 13 February 2024, date of current version 13 March 2024.

Digital Object Identifier 10.1109/ACCESS.2024.3365492

RESEARCH ARTICLE

Inverse Decoupling Fuzzy Active Disturbance Rejection Control for Supercritical CO_2 Extraction

MENGLONG CAO, ZHAOSEN ZHU, AND YUNPENG JU
College of Automation and Electronic Engineering, Qingdao University of Science and Technology, Qingdao 266100, China
Corresponding author: Yunpeng Ju (03297@qust.edu.cn)

This work was supported by the Natural Science Foundation of Shandong Province under Grant ZR2020KE037 and Grant ZR2020MF087.

ABSTRACT Aiming at the problem of strong coupling and time-delay issues in the temperature-pressure control of supercritical CO_2 extraction systems, an inverse decoupling fuzzy active disturbance rejection control method based on pole approximation is proposed. Firstly, by approximating the time-delay link of the controlled subsystem using pole approximation, the matching degree of the two-input signals of the linear extended state observer (LESO) is improved. Secondly, an inverse decoupling time-synchronized active disturbance rejection control method is proposed to address the coupling link of temperature-pressure as well as the complex control environments and numerous disturbances. Furthermore, the controller parameters are tuned using bandwidth method and fuzzy control rules, and theoretical analysis of this method is conducted. In addition, comparative simulations are conducted to validate this method against other approaches. The results indicate that this method exhibits better tracking performance, disturbance rejection capability, and robustness in the temperature-pressure control of supercritical CO_2 extraction systems. Finally, the feasibility of this method in reality was verified through experimental platforms.

INDEX TERMS CO_2 extraction, active disturbance rejection control, inverse decoupling, pole approximation, fuzzy control.

I. INTRODUCTION

Supercritical CO_2 extraction technology, known as ''green separation technique,'' allows for the efficient extraction of components from raw materials in an extraction environment with specific temperature, pressure, and CO_2 concentration. Compared to traditional organic solvent extraction techniques, supercritical CO_2 extraction technology offers advantages, such as high extraction efficiency, high economic value, and environmental friendliness. It is widely used in fields, such as pharmaceuticals, food, environmental protection, and fragrance industries [1]. As important parameters, the temperature and pressure in the supercritical CO_2 extraction process have strongly coupled and time-delay characteristics, which significantly affect the control performance and extraction efficiency [2], [3].

The associate editor coordinating the review of this manuscript and approving it for publication was Xiaojie Su.

Currently, most of the temperature and pressure control issues in supercritical CO_2 extraction systems are controlled separately using PID methods. This method ignores the coupling between temperature and pressure, and does not handle disturbances. The adjustment of control parameters mostly relies on the experience of operators. This method is difficult to accurately control temperature and pressure, especially when disturbances occur due to changes in the production environment.

Firstly, this article decouples the existing coupling terms through decoupling methods. Then, a control method is designed to control the decoupled object.

In order to address the issue of coupling between different controlled objects, the traditional single-variable control methods are difficult to apply directly. It is necessary to use decoupling methods to transform the multi-input multi-output (MIMO) system with coupling terms into multiple single-input single-output (SISO) systems.

Wang et al. proposed an active disturbance rejection decoupling method with online compensation, which considers the internal coupling of subsystems as part of the total disturbance and achieves decoupling control by extending the state observer estimation and compensating for the total disturbance, and applied this method to the independent measurement of electro-hydraulic servo systems in order to address the issues of strong coupling and time-varying parameters in the system [4]. Zhang et al. proposed a model-assisted self-disturbance control method, which utilizes a static decoupling matrix to decouple the coupling system of dual-input and dual-output, and designs a model-assisted extended state observer (ESO) for estimation and compensation to address the issue of interference between the two loops [5]. Li et al. proposed a synchronous robust decoupling output feedback control method for multivariable industrial processes with uncertain parameters, which the system transfer function was transformed into a nonsingular diagonal matrix, and the parameterized matrix, controller were designed using coprime factorization theory, and the feasibility of this method was verified by applying it to the control system of hot-rolled strip steel [6]. Shen et al. proposed an adaptive iterative control algorithm for intelligent decoupling control of the multi-zone temperature control in a large vertical quenching furnace, which constructs feature vectors and uses a self-updating recurrent neural network to adjust the control parameters of each control loop in real-time, achieving intelligent decoupling control of the temperature field [7]. Liu et al. proposed a control-model-based predictive control with feed-forward decoupling method and introduced a decentralized optimization strategy, which reduces the coupling degree of the system and the online computational workload for SISO or small-scale MIMO systems formed under extreme conditions [8]. Wu et al. proposed a decoupling control method based on inverse decoupling, which eliminates the coupling terms between channels, and achieves complete decoupling by introducing an inverse decoupling before the coupled objects with feedback ideas, greatly simplifying the complexity of the decoupling and being unaffected by the system's complexity [9].

For the problem of time-delay in the controlled object, the control performance of the controller is greatly limited. Hou et al. proposed an improved predictive PI control method by studying the principles of predictive PI controllers and combining them with the Smith disturbance rejection structure [10]. Adel et al. proposed a fractional order PID control method based on the immune feedback mechanism, which combines the control algorithm with fractional calculus and designs a new controller structure, and the controller parameters were tuned and optimized using a genetic algorithm [11]. Zhang and Wang proposed a finite time sliding mode control method to address the issues of time delay and uncertainty in the controlled object, which utilizes *Lyapunov* stability theory to analyze the finite time stability of the closed-loop system during both the arrival stage and sliding mode stage [12].

In the 1990s, Han and Zhang proposed an active disturbance rejection control (ADRC) technique based on PID control [13], [14]. Due to its real-time estimation and dynamic compensation performance, this control method has been widely applied in various uncertain systems. In order to reduce the workload of tuning parameters and simplify the control loop, GAO proposed a linear active disturbance rejection control (LADRC) method [15], [16], [17]. In LADRC, the presence of time-delay directly affects the synchronization degree of LESO's control output and output feedback on the time axis, which has a significant impact on the control effectiveness and performance of the LADRC. Zheng et al. proposed a predictive active disturbance rejection control method (SP-ADRC) that combines the Smith predictor with ADRC, and advances the estimation of the output feedback signal $y(t)$ of LESO. However, this method relies heavily on the accurate model of the controlled object [18]. Zhang et al. proposed a feed-forward compensation-based active disturbance rejection control method, which combines the advantages of Smith predictor and active disturbance rejection controller, and proves the asymptotic stability of the closed-loop control system through *Lyapunov* theory and input-output stability theory [19]. Zhao et al. proposed an improved Smith predictor-based active disturbance rejection control method (MSP-ADRC), which enhances the prediction performance of the Smith predictor by incorporating a feedback controller $T_c = (\sqrt{T/\tau})/K$ into the traditional Smith predictor [20]. Fatima et al. proposed a time-delayed active disturbance rejection controller based on predictive ESO, which compensates for disturbances caused by time-delay using a predictive approach, and combined an extended state observer with a delay-based ADRC method [21]. Bai et al. represented the effect of time delay as a transfer function and designed an ESO based on an predictor using partial differential equation back-stepping method, which also introduces a cascaded extended state observer structure [22].

To address the strong coupling and time-delay characteristics of temperature-pressure in supercritical CO_2 extraction systems, this paper proposes a pole-approximation-based inverse decoupling fuzzy active disturbance rejection control method. Firstly, by approximating and attenuating the time-delay link using pole approximation, the impact of time mismatch between the two input signals of the LESO is reduced. Secondly, by decoupling the coupling terms in the system through inverse decoupling, the system structure is simplified, leading to reduced computational burden. Thirdly, by combining the LADRC concept, a time-synchronized active disturbance rejection controller is designed. This approach can eliminate the impact of uncertain external disturbances on the control system. In addition, the stability and robustness of this approach are analyzed and verified. Lastly, the parameter tuning method is determined using the bandwidth method, and the controller parameters are optimized through fuzzy control. This method ensures that the

temperature and pressure control in the supercritical CO_2 extraction system achieve satisfactory control performance.

II. SUPERCRITICAL CO_2 EXTRACTION MODEL AND TIME-DELAY APPROXIMATION

A. SUPERCRITICAL CO_2 EXTRACTION PROCESS

The structure of the supercritical CO_2 extraction process is shown in Figure 1. Its principle is based on the excellent solubility of CO_2 with certain natural substances. In the supercritical state, CO_2 exhibits excellent permeability and solubility towards materials. By fully contacting the supercritical CO_2 with the substances to be separated, it selectively extracts components of different polarities, boiling points, and molecular weights [23]. Then, by using methods, such as depressurization and temperature adjustment, the extracted substances are precipitated to achieve the purpose of separation and purification. Near the critical point, even small changes in pressure or temperature can cause significant changes in fluid density, resulting in corresponding changes in solubility. Temperature and pressure inside the extraction vessel are the primary factors that significantly influence the extraction efficiency during the extraction process. During the extraction process, it is necessary to strictly control the state of CO_2 and minimize the impact of temperature-pressure instability during the control process on the extraction rate.

FIGURE 1. Structure diagram of supercritical CO_2 extraction.

As the primary influencing factors during the extraction process, the appropriate temperature and stable pressure inside the extraction vessel play a crucial role in the extraction effectiveness and efficiency. As a solvent, CO_2 has higher requirements for temperature and pressure in terms of gas viscosity, thermal conductivity, and heat of fusion. This leads to a coupling relationship between temperature and pressure in a CO_2 extraction system.

The process of supercritical CO_2 extraction is as follows:

- The material to be extracted is placed into the extraction vessel E, and then the CO_2 from the CO_2 storage tank GT is compressed into the extraction vessel E through the compressor MC, providing a stable pressure environment for CO_2 extraction.
- The heating tube HE and the super thermostatic controller UT provide a suitable temperature environment for CO_2 extraction.
- CO_2 is stabilized in a supercritical state, allowing it to fully contact with the material to be extracted and carry out the extraction process.
- After the extraction is complete, the pressure inside the extraction vessel is balanced to atmospheric pressure by opening the pressure relief valve RV3. Then, the extracted material is taken out.

The supercritical CO_2 extraction process is shown in Figure 2.

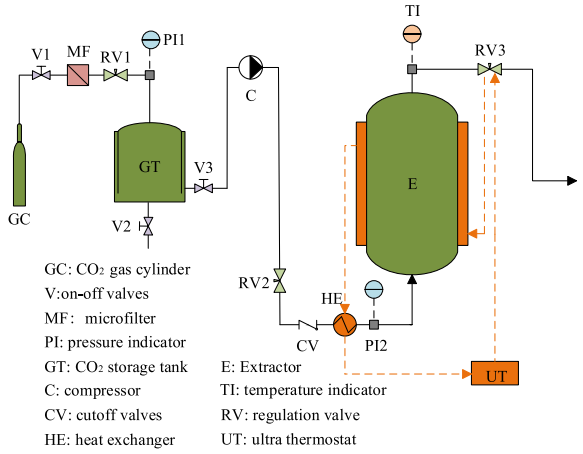

FIGURE 2. Process diagram supercritical CO_2 extraction.

B. SUPERCRITICAL CO_2 EXTRACTION MODEL

The precise and stable control of temperature and pressure is crucial for achieving high efficiency, low energy consumption, and high extraction yield in the supercritical CO_2 extraction process. According to [24], the temperature-pressure model of the extraction vessel can be described as a first-order inertia process with a lag element. Establish a coupling model of temperature-pressure inside the extraction vessel using the Peng-Robinson (PR) equation for CO_2 in its critical state. The PR equation is as follows [24]:

$$\left.\begin{aligned} \frac{RT}{V-b}-\frac{a(T)}{V(V+b)+b(V-b)}&=P\\ a(T_c)\alpha&=a(T)\\ 0.45724\frac{R^2T_c^2}{P_c}&=a(T_c)\\ 1.7075e^{-0.5376T/T_C}&=\alpha\\ 0.0778\frac{RT_c}{P_c}&=b \end{aligned}\right\} \tag{1}$$

In equation (1), a-cohesion parameter; b- co-volume parameter; R- gas constant, $8.3145J.mol^{-1}.k^{-1}$; α- correlation for CO_2 critical state; V- molar volume of CO_2; T - temperature, K; T_c - critical temperature, $304.2K$; P - pressure, MPa; P_c - critical pressure, $7.38MPa$.

According to [24], through mechanistic modeling, the coupling model of temperature-pressure in supercritical CO_2

extraction is represented as follows:

$$\begin{bmatrix} y_1(s) \\ y_2(s) \end{bmatrix} = \begin{bmatrix} G_{11}(s) & G_{12}(s) \\ G_{21}(s) & G_{22}(s) \end{bmatrix} \begin{bmatrix} r_1(s) \\ r_2(s) \end{bmatrix} = \begin{bmatrix} \frac{1.2}{15s+1}e^{-37s} & \frac{0.0115}{15s+1}e^{-37s} \\ \frac{0.027}{4.26s+1}e^{-45s} & \frac{0.27}{4.26s+1}e^{-45s} \end{bmatrix} \begin{bmatrix} r_1(s) \\ r_2(s) \end{bmatrix} \tag{2}$$

In equation (2), $y_1(s)$ represents the temperature inside the extraction vessel, $y_2(s)$ represents the pressure inside the extraction vessel, $r_1(s)$ represents the heating time of the electric heating tube, and $r_2(s)$ represents the rotational speed of the pressurized pump motor.

C. APPROXIMATION OF THE POLE OF THE TIME-DELAY LINK

In LADRC, when the controlled object has a time-delay link, the output feedback $y(t-\tau)$ of the control system and the control input $y(t)$ are lagged by τ in the time axis, which causes the two input signals of the LESO to be out of synchronization in time. This seriously affects the observation accuracy and effectiveness of the LESO, resulting in poor control performance of the control system [25]. In particular, when the system is subjected to external disturbances or the controlled object exhibits uncertainty, the LADRC cannot immediately and effectively handle the disturbances and uncertainties, resulting in its control effectiveness not being fully realized. For a controlled object with time-delay link, due to the poor observation effectiveness of the LESO, there is a need for excessive pursuit of system stability and compensation gain b_0 to improve the system's stability margin. However, this can impact the quick response of control effectiveness. Moreover, when $n = b_0/b$ is too large, the stable region of ω_0 and ω_c in the plane will decrease. In other words, the range of values for ω_0 and ω_c when the system is stable will be reduced, which is not conducive to tuning the parameters of the controller.

In response to the issue of mismatched time signals of the two-input signals for the LESO, the LADRC based on Smith predictor theoretically solves the problem of output feedback time-delay. When there is uncertainty or parameter perturbation in the controlled object, the control quality may not achieve the desired results. With the research and application of some intelligent algorithms, some scholars have combined these algorithms with traditional control methods, proposing improved control methods optimized by intelligent algorithms. However, this method has a high level of system complexity and has high requirements for operating speed and accuracy, making it difficult to apply in practice [26], [27].

To address the time-delay issue of the controlled object, this article approximates the time-delay link by using the pole approximation method as follows:

$$e^{-\tau s} \approx L_m = 1/(\frac{1}{2}\tau^2 s^2 + \tau s + 1) \tag{3}$$

This article selects the temperature control channel as the controlled object and approximates the time-delay link using three different methods: first-order Taylor expansion approximation, first-order Pade approximation, and pole approximation. The approximations are shown in Figure 3. In the initial approximation, both first-order Taylor expansion approximation and first-order Pade approximation exhibit approximate oscillations. However, the early rising response of the first-order Taylor expansion approximation is not accurate enough for approximating the time-delay link. The approximation curve of the pole approximation method is relatively smooth, with minimal approximation oscillations. It provides a better approximation effect compared to other methods.

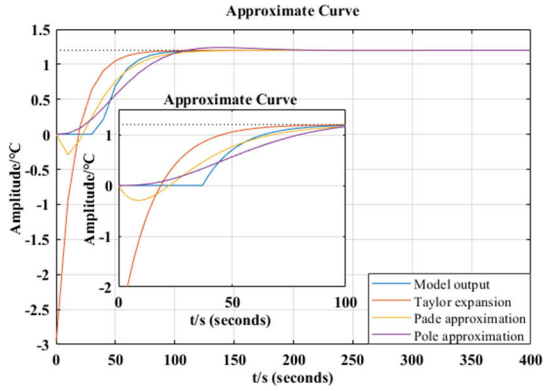

FIGURE 3. Comparison of approximate effects.

III. INVERSE DECOUPLING FUZZY ADRC METHOD

A. DESIGN OF INVERSE DECOUPLING CONTROLLER

For a MIMO system, there are coupling terms between the subsystems, which significantly affect the control effectiveness of the controller for each subsystem. Consider the following MIMO system:

$$\begin{bmatrix} y_1 \\ y_2 \\ \vdots \\ y_n \end{bmatrix} = \begin{bmatrix} G_{11} & G_{12} & \cdots & G_{1n} \\ G_{21} & G_{22} & \cdots & G_{2n} \\ \vdots & \vdots & \ddots & \vdots \\ G_{n1} & G_{n2} & \cdots & G_{nn} \end{bmatrix} \begin{bmatrix} u_1 \\ u_2 \\ \vdots \\ u_n \end{bmatrix} \tag{4}$$

Design an inverse decoupling controller for the system as follows:

$$D(s) = \begin{bmatrix} 0 & D_{12} & \cdots & D_{1n} \\ D_{21} & 0 & \cdots & D_{2n} \\ \vdots & \vdots & \ddots & \vdots \\ D_{n1} & D_{n2} & \cdots & 0 \end{bmatrix} = \begin{bmatrix} 0 & -\frac{G_{12}}{G_{11}} & \cdots & -\frac{G_{1n}}{G_{11}} \\ -\frac{G_{21}}{G_{22}} & 0 & \cdots & -\frac{G_{2n}}{G_{22}} \\ \vdots & \vdots & \ddots & \vdots \\ -\frac{G_{n1}}{G_{nn}} & -\frac{G_{n2}}{G_{nn}} & \cdots & 0 \end{bmatrix} \tag{5}$$

Let's denote it as:

$$\begin{bmatrix} u_1 \\ u_2 \\ \vdots \\ u_n \end{bmatrix} = \begin{bmatrix} r_1 \\ r_2 \\ \vdots \\ r_n \end{bmatrix} + \begin{bmatrix} 0 & D_{12} & \cdots & D_{1n} \\ D_{21} & 0 & \cdots & D_{2n} \\ \vdots & \vdots & \ddots & \vdots \\ D_{n1} & D_{n2} & \cdots & 0 \end{bmatrix} \begin{bmatrix} u_1 \\ u_2 \\ \vdots \\ u_n \end{bmatrix} \tag{6}$$

Then, we have:

$$\begin{bmatrix} u_1 \\ u_2 \\ \vdots \\ u_n \end{bmatrix} = \begin{bmatrix} 1 & -D_{12} & \cdots & -D_{1n} \\ -D_{21} & 1 & \cdots & -D_{2n} \\ \vdots & \vdots & \ddots & \vdots \\ -D_{n1} & -D_{n2} & \cdots & 1 \end{bmatrix}^{-1} \begin{bmatrix} r_1 \\ r_2 \\ \vdots \\ r_n \end{bmatrix} \tag{7}$$

After the inverse decoupling, a MIMO system with coupling terms can be transformed into completely decoupled multiple SISO subsystems. The decoupled controlled system can be expressed as:

$$\begin{aligned} \begin{bmatrix} y_1 \\ y_2 \\ \vdots \\ y_n \end{bmatrix} &= \begin{bmatrix} G_{11} & G_{12} & \cdots & G_{1n} \\ G_{21} & G_{22} & \cdots & G_{2n} \\ \vdots & \vdots & \ddots & \vdots \\ G_{n1} & G_{n2} & \cdots & G_{nn} \end{bmatrix} \\ &\times \begin{bmatrix} 1 & -D_{12} & \cdots & -D_{1n} \\ -D_{21} & 1 & \cdots & -D_{2n} \\ \vdots & \vdots & \ddots & \vdots \\ -D_{n1} & -D_{n2} & \cdots & 1 \end{bmatrix}^{-1} \begin{bmatrix} r_1 \\ r_2 \\ \vdots \\ r_n \end{bmatrix} \\ &= \begin{bmatrix} G_{11} & 0 & \cdots & 0 \\ 0 & G_{22} & \cdots & 0 \\ \vdots & \vdots & \ddots & \vdots \\ 0 & 0 & \cdots & G_{nn} \end{bmatrix} \begin{bmatrix} r_1 \\ r_2 \\ \vdots \\ r_n \end{bmatrix} \end{aligned} \tag{8}$$

The decoupling of the coupling model by the inverse decoupling is achieved by dividing the coupling terms between the coupling models by the transfer functions of the subsystems. This is done to avoid the following situations [28]:

- When the time delay in the denominator is larger than that in the numerator, the decoupling function will have advanced time terms.
- When the numerator order of the decoupling function is higher than the denominator order, prediction terms will appear.
- The inverse decoupling contains unstable zeros, which may cause the decoupled subsystems to be unstable.

Therefore, before designing the inverse decoupling, it is necessary to compensate for the controlled object in order to address the aforementioned issues. For industrial controlled objects with many external influencing factors, it is easy to have inaccurate identification of the controlled object and parameter perturbations, which inevitably introduces certain uncertainties in the object. These errors can be treated as total disturbances and observed and compensated by LESO to achieve stable control of the system. The inverse decoupling control structure for the temperature-pressure coupling model of supercritical CO_2 extraction is shown in Figure 4.

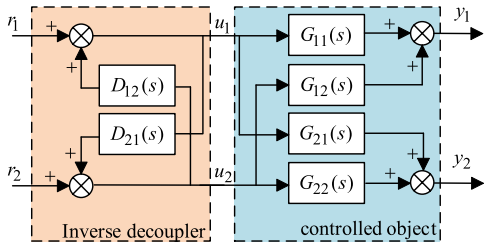

FIGURE 4. Diagram of the inverse decoupling control structure.

After decoupling through an inverse decoupler, the original controlled object is decoupled into

$$\begin{aligned} \begin{bmatrix} y_1 \\ y_2 \end{bmatrix} &= \begin{bmatrix} G_{11} & 0 \\ 0 & G_{22} \end{bmatrix} \begin{bmatrix} r_1 \\ r_2 \end{bmatrix} \\ &= \begin{bmatrix} \dfrac{1.2}{15s+1} e^{-37s} & 0 \\ 0 & \dfrac{0.27}{4.26s+1} e^{-45s} \end{bmatrix} \begin{bmatrix} r_1 \\ r_2 \end{bmatrix} \end{aligned} \tag{9}$$

B. TIME-SYNCHRONIZED ADRC METHOD

In LADRC, it is generally assumed that the mathematical model of the controlled object is

$$y^{(n)}(t) = bu(t) + f(y^{(n-1)}(t), \ldots, y(t), u(t), w(t)) \tag{10}$$

In equation (10), n represents the system order, b represents the system high-frequency gain, $f(y^{(n-1)}(t), \ldots, y(t), u(t), w(t))$ represents the total disturbance of the system, and $w(t)$ represents the external disturbance.

The core of linear active disturbance rejection control is to use a linear extended state observer (LESO) to estimate the total disturbance of the system. Equation (10) can be converted into state-space form as follows:

$$\begin{cases} x_1(t) = y(t) \\ x_2(t) = \dot{y}(t) \\ \vdots \\ x_n(t) = y^{(n-1)}(t) \\ x_{n+1}(t) = f(y(t), u(t), w(t)) \end{cases} \tag{11}$$

Assuming that the total disturbance of the system, denoted as f, is bounded and differentiable, the augmented state equation of the original system is given by:

$$\begin{cases} \dot{X} = AX + Bu + E\dot{f} \\ y = CX \end{cases} \tag{12}$$

In equation (12),

$$X = [x_1(t), x_2(t), \cdots, x_{n+1}(t)]^{\mathrm{T}},$$

$$A = \begin{bmatrix} 0 & 1 & 0 & \cdots & 0 \\ 0 & 0 & 1 & \cdots & 0 \\ \vdots & \vdots & \vdots & \ddots & \vdots \\ 0 & 0 & 0 & \cdots & 1 \\ 0 & 0 & 0 & \cdots & 0 \end{bmatrix}_{(n+1)(n+1)},$$

$$B = \begin{bmatrix} 0 & 0 & \cdots & b & 0 \end{bmatrix}^{\mathrm{T}}_{(n+1)\times 1},$$

$$E = \begin{bmatrix} 0 & 0 & \cdots & 0 & 1 \end{bmatrix}^{\mathrm{T}}_{(n+1)\times 1},$$

$$C = \begin{bmatrix} 1 & 0 & \cdots & 0 & 0 \end{bmatrix}_{1\times(n+1)}.$$

Based on the above object, the expression for designing a LESO is as follows:

$$\begin{cases} \dot{Z} = AZ + Bu + L(y - z_1) \\ z_1 = CZ \end{cases} \tag{13}$$

In equation (13), $Z = \begin{bmatrix} z_1 & z_2 & \cdots & z_{n+1} \end{bmatrix}^{\mathrm{T}}$ is the observation matrix of the state variable X, and $L = \begin{bmatrix} \beta_1 & \beta_2 & \cdots & \beta_{n+1} \end{bmatrix}^{\mathrm{T}}$ is the gain parameter matrix of the observer.

The linear error feedback control law (LSEF) is

$$\begin{aligned} u(t) &= \frac{k_1(r - z_1) + \cdots + k_n(r^{(n-1)} - z_n) - z_{n+1}}{b_0} \\ &= K_c(R - Z) \end{aligned} \tag{14}$$

In equation (14), $K_c = \begin{bmatrix} k_1 & k_2 & \cdots & k_n & 1 \end{bmatrix}/b_0$ represents the state feedback gain, b_0 represents the estimation of b, and $R = \begin{bmatrix} r & \dot{r} & \cdots & r^{(n-1)} & 0 \end{bmatrix}^{\mathrm{T}}$ represents the reference input.

For control systems with large time delays, this paper approximates the time delay element using pole approximation and designs a time-synchronized ADRC as shown in Figure 5.

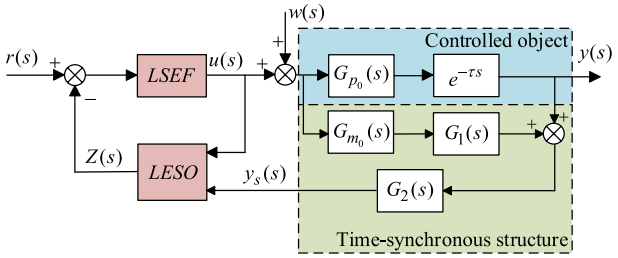

FIGURE 5. Time-synchronous ADRC.

In Figure 5, $G_1(s) = (l^2 - 1)L_m$, $G_2(s) = 1/\{[\tau_m(l-1)s + l^2 - 1]L_m + 1\}$. By introducing a time-synchronized structure, the output feedback matrix A of the extended state observer is transformed into

$$\begin{aligned} y_s(t) &= (G_{p_0}(s)e^{-\tau s} + G_{m_0}(s)G_1(s))G_2(s) \\ &= \frac{G_{p_0}(s)e^{-\tau s} + G_{m_0}(s)(l^2 - 1)L_m}{[\tau(l-1)s + l^2 - 1]L_m + 1} \end{aligned} \tag{15}$$

In equation (15), $G_{m_0}(s)$ represents the model estimation of the actual controlled object $G_{p_0}(s)$, and l represents the time synchronization factor.

If $G_{m_0}(s) = G_{p_0}(s)$ and $\tau_m = \tau$. If we approximate the time delay element of the controlled object by pole approximation, denoted as $e^{-\tau s} \approx L_m$, then

$$y_s(t) = G_{p_0}(s)\frac{1}{\frac{1}{2}\frac{\tau^2}{l^2}s^2 + \frac{\tau}{l}s + 1} = G_{p_0}(s)e^{-\frac{\tau}{l}s} \tag{16}$$

In theory, the larger the time synchronization factor l, the higher the degree of time matching between the control output $u(t)$ and the system output $y(t)$. When selecting the time synchronization factor l, it is sufficient to ensure that the degree of time synchronization meets the control requirements. There is no need to excessively pursue a larger value of l, as it may increase practical burdens without significant benefits. Based on extensive simulation analysis, it is generally recommended to set $l \geq (2 \sim 5)^{n+1}\tau/T$ to the order of the controlled object, n represents the order of the controlled object. When the time delay is large, a larger value of l is usually selected.

By designing a time synchronization structure, the time-delay coefficient τ of a system with time-delay is reduced to the value of τ/l. This helps to decrease the degree of temporal mismatch between the two input signals of the LESO in the time domain. In actual industrial production processes, it is impossible for the system model and parameters to be completely identical. At the same time, the time synchronization structure approximates the time-delay link of the controlled object twice, which inevitably introduces some level of uncertainty in the object. These errors can be treated as total disturbances and observed and compensated for by LESO to achieve stable control of the system.

C. TUNING RULES FOR PARAMETERS

The selection of controller parameters is crucial for ensuring system stability and satisfactory dynamic performance. The parameters of the time-synchronized active disturbance rejection controller mainly include the system stability and compensation gain b_0, observer gain parameter $[\beta_1, \beta_2, \cdots, \beta_{n+1}]$, controller gain parameter $[k_1, k_2, \cdots, k_n]$, and time synchronization factor l. The observer gain parameter and the controller gain parameter are tuned using the bandwidth method, which means that

$$\begin{cases} \beta_i = C_{n+1}^i \omega_0^i & (i = 1, 2, \ldots, n+1) \\ k_i = C_n^i \omega_c^i & (i = 1, 2, \ldots, n) \end{cases} \tag{17}$$

In equation (17), n represents the order of the controlled object, ω_c represents the controller bandwidth, and ω_0 represents the observer bandwidth. The tuning rules for the parameters of system stability and compensation gain b_0, controller bandwidth ω_c, observer bandwidth ω_0, and time synchronization factor l are as follows.

The system stability and compensation gain b_0 is an important parameter that affects the stability of the system. By adjusting b_0, the system can have better stability performance. Generally, it is advisable to choose an appropriate compensation gain $b_0 = nb$. Increasing n will result in a

greater stability margin for the system, but at the expense of decreased system speed. Additionally, the stable region in the plane for controller bandwidth ω_c and observer bandwidth ω_0 will decrease, which is not conducive to parameter selection and tuning. When there is a time-delay link in the controlled object, it is necessary to choose a larger value for compensation gain n to ensure system stability. Generally, n is chosen to be $2 \sim 8$. ω_c is the primary parameter that affects the system's settling time. By adjusting ω_c, a satisfactory settling time can be achieved. $\omega_c = m a$, as m increases, the system's response speed improves, but its anti-noise ability decreases, which can lead to system oscillation. The $m = 1 \sim 3$ is generally chosen. ω_0 affects the overall performance of the system by influencing the observation performance of LESO. $\omega_0 = c\omega_0$, as c increases, the overshoot of the system output decreases, but it also leads to a decrease in the system's response speed. Additionally, it makes the system more sensitive to parameter perturbations in the controlled system. The $c = 2 \sim 5$ is generally chosen.

When the time synchronization factor l is larger, the control output $u(t)$ and the system output $y(t)$ have a higher degree of time matching. For the selection of the time synchronization factor l, it is sufficient to have a degree of time synchronization that satisfies the control requirements, and there is no need to excessively pursue a larger value that may increase the burden on the system. After extensive simulation analysis, it is generally recommended to choose a suitable value for $l \geq (2 \sim 5)^{n+1}\tau/T$. n is typically determined based on the order of the controlled object. When dealing with systems with significant time delays, it is often advisable to select a larger value for l to ensure proper compensation for the delay.

D. FUZZY CONTROL RULES

The LSEF is the key to ensuring smooth convergence of the system, but it weakens the system's anti-interference ability and robustness. Fuzzy controllers have the advantages of improving system robustness and control accuracy, as well as realizing parameter self-tuning. In order to improve the adaptive ability of the controller to pressure-temperature control, this paper combines the characteristics of LADRC and fuzzy control to further improve the control performance of the system, in order to achieve better control effect. Design a fuzzy ADRC as shown in Figure 6.

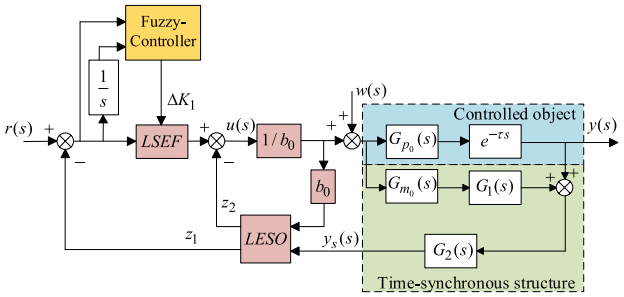

FIGURE 6. Fuzzy ADRC structure diagram.

Designing a fuzzy robust control controller for tuning control parameter K_1, that

$$K_1 = K_1^b + \beta \Delta K_1 \tag{18}$$

In equation (18), K_1^b represents the baseline value of K_1, β represents the adjustment slope of K_1, ΔK_1 represents the adjustment variable. Determine the value of ΔK_1 using the following Mamdani-type fuzzy inference, which means

$$R_j: \text{ IF } x_1 \text{ is } X_1^i \text{ AND } x_2 \text{ is } X_2^j, \text{ THEN } \Delta K_1 \text{ is } F^{ij} \tag{19}$$

In equation (19), R_j represents the j-th rule (out of a total of 49 rules), $X_1^i (i = 1, 2, \cdots, 7)$ represents the fuzzy set of input variable x_1; $X_2^j (j = 1, 2, \cdots, 7)$ represents the fuzzy set of input variable x_2; F^{ij} represents the fuzzy set of output variable ΔK_1.

Using fuzzy inference, the output of the fuzzy controller is obtained as

$$\hat{f}(x) = \frac{\sum_{i=1}^{7}\sum_{j=1}^{7} y^{ij}\left(\prod_{i=1,j=1}^{2} \mu_{X_1^i}(x_1)\mu_{X_2^j}(x_2)\right)}{\sum_{i=1}^{7}\sum_{j=1}^{7}\left(\prod_{i=1,j=1}^{2} \mu_{X_1^i}(x_1)\mu_{X_2^j}(x_2)\right)} \tag{20}$$

The fuzzy controller designed in this paper takes the error E between the setpoint and the observed value, as well as the rate of change of the error EC, as inputs, and outputs the controller parameter ΔK_1. To improve control effectiveness and maximize the advantages of fuzzy control, the fuzzy domain is selected as $\{-1.5, -1, -0.5, 0, 0.5, 1, 1.5\}$, and 7 fuzzy subsets are used to describe the input and output, namely {NB, NM, NS, ZO, PS, PM, PB}. Design fuzzy rules as shown in Table 1.

TABLE 1. Fuzzy rule table.

EC	E						
	NB	NM	NS	ZO	PS	PM	PB
NB	NB	NB	NB	NB	NM	NM	NS
NM	NB	NB	NB	NM	NS	ZO	ZO
NS	NB	NB	NM	NS	ZO	ZO	ZO
ZO	NB	NM	NS	ZO	PS	PM	PB
PS	ZO	ZO	ZO	PS	PM	PB	PB
PM	ZO	ZO	PS	PM	PB	PB	PB
PM	PS	PM	PB	PB	PB	PB	PB

IV. STABILITY AND ROBUSTNESS ANALYSIS

A. STABILITY ANALYSIS

Let $G_{p0}(s) = b/(s + a)$ be a first-order controlled object. $G_m(s) = b_m/(s + a_m)$ is the model estimation of the actual controlled object $G_{p_0}(s)$. The transfer function of the

time-synchronous ADRC using LESO is given by

$$\begin{cases} z_1 = \dfrac{\beta_1 s+\beta_2}{s^2+\beta_1 s+\beta_2}\dfrac{y+(l^2-1)L_m G_m u}{[\tau_m(l-1)s+l^2-1]L_m+1} \\ \qquad +\dfrac{bs}{s^2+\beta_1 s+\beta_2}u \\ z_2 = \dfrac{\beta_2 s}{s^2+\beta_1 s+\beta_2}\dfrac{y+(l^2-1)L_m G_m u}{[\tau_m(l-1)s+l^2-1]L_m+1} \\ \qquad -\dfrac{\beta_2 b}{s^2+\beta_1 s+\beta_2}u \end{cases} \tag{21}$$

Design a first-order LSEF as

$$u=\frac{k_1(r-z_1)-z_2}{b} \tag{22}$$

By combining equations (21) and (22), it can be concluded that

$$u=\frac{(s^2+\beta_1 s+\beta_2)P(s)}{[bs^2+b(\beta_1+k_1)s]P(s)+[(k_1\beta_1+\beta_2)s+k_1\beta_2](l^2-1)G_m L_m} \cdot\left[k_1 r-\frac{(k_1\beta_1+\beta_2)s+k_1\beta_2}{(s^2+\beta_1 s+\beta_2)P(s)}y\right] \tag{23}$$

In equation (23), $P(s)=[\tau_m(l-1)s+l^2-1]L_m+1$.

According to equation (23), the closed-loop feedback structure of the time synchronous ADRC is shown in Figure 7.

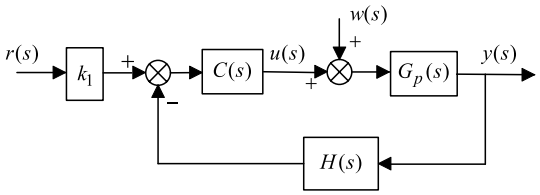

FIGURE 7. Closed loop feedback structure of ADRC.

In Figure 7,

$$C(s)=\frac{(s^2+\beta_1 s+\beta_2)\{[\tau_m(l-1)s+l^2-1]L_m+1\}}{[bs^2+b(\beta_1+k_1)s]P(s)+[(k_1\beta_1+\beta_2)s+k_1\beta_2](l^2-1)G_m L_m} \tag{24}$$

$$H(s)=\frac{(k_1\beta_1+\beta_2)s+k_1\beta_2}{(s^2+\beta_1 s+\beta_2)P(s)} \tag{25}$$

The open-loop transfer function of the first-order time synchronous ADRC is

$$G(s)=C(s)H(s)G_{p_0}(s)e^{-\tau s} \tag{26}$$

When $l=1$, that is, without introducing the time-synchronous link, the open-loop transfer function of the system is given by

$$G(s)=\frac{(k_1\beta_1+\beta_2)s+k_1\beta_2}{b[s^2+(\beta_1+k_1)s]}G_{p_0}(s)e^{-\tau s} \tag{27}$$

The corresponding open-loop poles are $s_1=0$ and $s_2=-(\beta_1+k_1)$. It can be inferred that the system is stable.

When introducing the time-synchronous link, the open-loop transfer function of the system is given by

$$\begin{aligned} G(s)[(k_1\beta_1+\beta_2)s+k_1\beta_2]/\{&bl\tau_m s^3+bl[\tau_m(\beta_1+k_1)+l]s^2 \\ &+l^2[b(\beta_1+k_1)+(k_1\beta_1+\beta_2)b_m/a_m]s \\ &+l^2 k_1\beta_2 b_m/a_m\}G_{p0}(s)e^{-\tau s} \end{aligned} \tag{28}$$

Its characteristic equation is

$$D(s)=d_0 s^3+d_1 s^2+d_2 s+d_3=0 \tag{29}$$

In equation (29),

$$\begin{aligned} d_0&=bl\tau_m \\ d_1&=bl[\tau_m(\beta_1+k_1)+l] \\ d_2&=[l^2 b(\beta_1+k_1)+(k_1\beta_1+\beta_2)(l^2 b_m/a_m+1)] \\ d_3&=k_1\beta_2(l^2 b_m/a_m+1) \end{aligned}$$

The main and sub equations of the coefficient determinant are

$$\begin{aligned} D_1&=d_1=bl[\tau_m(\beta_1+k_1)+l] \\ D_2&=\begin{vmatrix} d_1 & d_3 \\ d_0 & d_2 \end{vmatrix}=bl\{[\tau_m(k_1+\beta_1)+l][l^2 b(k_1+\beta_1) \\ &\quad +k_1\beta_1(\frac{l^2 b_m}{a_m}+1)]+\beta_2(\tau_m\beta_1+l)(\frac{l^2 b_m}{a_m}+1)\} \\ D_3&=\begin{vmatrix} d_1 & d_3 & 0 \\ d_0 & d_2 & 0 \\ 0 & d_1 & d_3 \end{vmatrix}=blk_1\beta_2(\frac{l^2 b_m}{a_m}+1) \\ &\quad \{[\tau_m(k_1+\beta_1)+l][l^2 b(k_1+\beta_1)+k_1\beta_1(\frac{l^2 b_m}{a_m}+1)] \\ &\quad +\beta_2(\tau_m\beta_1+l)(\frac{l^2 b_m}{a_m}+1)\} \end{aligned}$$

In the time-synchronous ADRC, the system parameters l, b, τ_m, k_1, β_1, β_2, a_m, and b_m are all positive. Then, $d_0>0$, $D_n>0$. From the *Routh-Hurwitz* criterion, it can be concluded that the system is stable.

B. ROBUSTNESS ANALYSIS

To analyze the robustness of time-synchronous ADRC, let's consider the controlled object $G_P=G_m(1+\Delta G_P)$. Here, G_m is the nominal model of the controlled object, and ΔG_P is the perturbation of the nominal model. And meet $|\Delta G_P(j\omega)|\le\overline{\Delta G_P(\omega)}$. $\overline{\Delta G_P(\omega)}$ is the bounded uncertainty of the multiplication norm.

For the traditional ADRC, it can be transformed into a closed-loop single feedback structure as shown in Figure 7. The open-loop transfer function can be obtained as follows

$$\overline{M}=(C(s)H(s))_1=\frac{(k_1\beta_1+\beta_2)s+k_1\beta_2}{b[s^2+(\beta_1+k_1)s]} \tag{30}$$

The characteristic equation of LADRC is given by

$$1+\overline{M}(G_m(1+\Delta G_P))=0 \tag{31}$$

According to the robust stability criterion, for any ω, the following equation can hold true.

$$\overline{\Delta G_P(\omega)}_1<dG_{p_1}(s)=\left|\frac{1+\overline{M}G_m}{\overline{M}G_m}\right|=\left|\frac{1}{\overline{M}G_m}+1\right| \tag{32}$$

For time-synchronous ADRC, the open-loop transfer function is given by

$$(C(s)H(s))_2 = [(k_1\beta_1 + \beta_2)s + k_1\beta_2](\frac{1}{2}\tau_m^2 s^2 + \tau_m s + 1)/ \{b[s^2 + (\beta_1 + k_1)s](\frac{1}{2}\tau_m^2 s^2 + \tau_m l s + l^2) + [(k_1\beta_1 + \beta_2)s + k_1\beta_2](l^2 - 1)G_m\} \quad (33)$$

Simplified results,

$$(C(s)H(s))_2 = \frac{(\frac{1}{2}\tau_m^2 s^2 + \tau_m s + 1)\overline{M}}{(\frac{1}{2}\tau_m^2 s^2 + \tau_m l s + l^2) + \overline{M}(l^2 - 1)G_m} = \delta\overline{M} \quad (34)$$

In equation (34),

$$\delta = \frac{(\frac{1}{2}\tau_m^2 s^2 + \tau_m s + 1)}{(\frac{1}{2}\tau_m^2 s^2 + \tau_m l s + l^2) + \overline{M}(l^2 - 1)G_m} < 1$$

Its characteristic equation is

$$1 + \overline{M}\delta(G_m(1 + \Delta G_P)) = 0 \quad (35)$$

According to the robust stability criterion, for any ω, the following equation can hold true.

$$\overline{\Delta G_P(\omega)}_2 < dG_{p_2}(s) = \left|\frac{1+\delta\overline{M}G_m}{\delta\overline{M}G_m}\right| = \left|\frac{1}{\delta\overline{M}G_m} + 1\right| \quad (36)$$

Comparing equation (32) and equation (36), we can observe that $dG_{p_2}(s) > dG_{p_1}(s)$. Time-synchronous ADRC allows for a larger perturbation bound compared to traditional ADRC, exhibiting stronger tolerance to parameter perturbations and enhanced robustness.

V. SIMULATION ANALYSIS

For the temperature-pressure coupling model in supercritical CO_2 extraction, the fuzzy pole-approximation-based inverse decoupling control method (FP-ADRC) is employed to control the coupling model. And a comparative analysis is conducted with traditional ADRC method, SP-ADRC method proposed by Zhang et al. [19], and MSP-ADRC method proposed by Zhao [20]. To ensure a fair comparison, this method selects the same bandwidth parameters as the SP-ADRC and MSP-ADRC methods. The parameters of the controllers for temperature control channel y_1 and pressure control channel y_2 are shown in Table 2.

TABLE 2. The parameters of the controllers.

	Controller	ω_c	ω_0	b_0	$l(T_c)$
y_1	ADRC	0.067	0.133	0.32	-
	SP-ADRC	0.13	0.26	0.08	-
	MSP-ADRC	0.13	0.26	0.08	0.53
	FP-ADRC	0.13	0.26	0.08	50
y_2	ADRC	0.23	0.46	0.317	-
	SP-ADRC	0.23	0.37	0.063	-
	MSP-ADRC	0.23	0.37	0.063	1.14
	FP-ADRC	0.23	0.37	0.063	200

A. SYSTEM RESPONSE OF IDEAL MODEL

Assuming that the model of the controlled system is accurate, a unit step input signal is applied to the four control methods, and a disturbance with an amplitude of -0.5 is introduced at point $t = 100s$. The unit step response of temperature control channel y_1 and pressure control channel y_2 are shown in Figures 8 and 9, respectively.

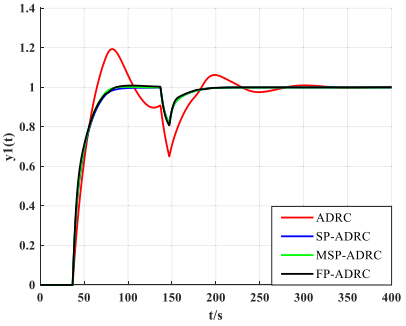

FIGURE 8. The unit step response of temperature control channel y_1.

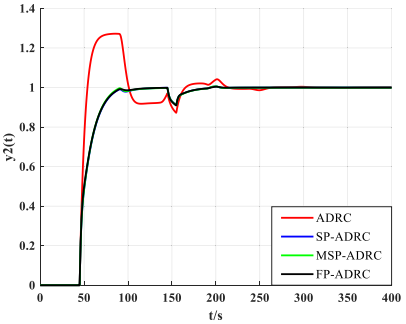

FIGURE 9. The unit step response of pressure control channel y_2.

From Figures 8 and 9, it can be observed that the traditional ADRC method has a significant overshoot and exhibits larger fluctuations when the system is disturbed. This is due to the impact of time-delay on the observing performance of LESO. The SP-ADRC and MSP-ADRC methods rely on the Smith predictor to accurately estimate the controlled object. They exhibit good response speed, tracking performance, and disturbance rejection capability for the temperature-pressure model of supercritical CO_2 extraction. The control effectiveness is similar to the proposed FP-ADRC method in this paper.

B. SYSTEM RESPONSE UNDER PARAMETER PERTURBATION

In practical production processes, it is not possible to accurately estimate the temperature and pressure model of supercritical CO_2 extraction. Especially in industrial production with complex environmental factors, the system parameters and model parameters of the controlled object may be subject to certain perturbations. The control effects of the four control methods under parameter perturbation

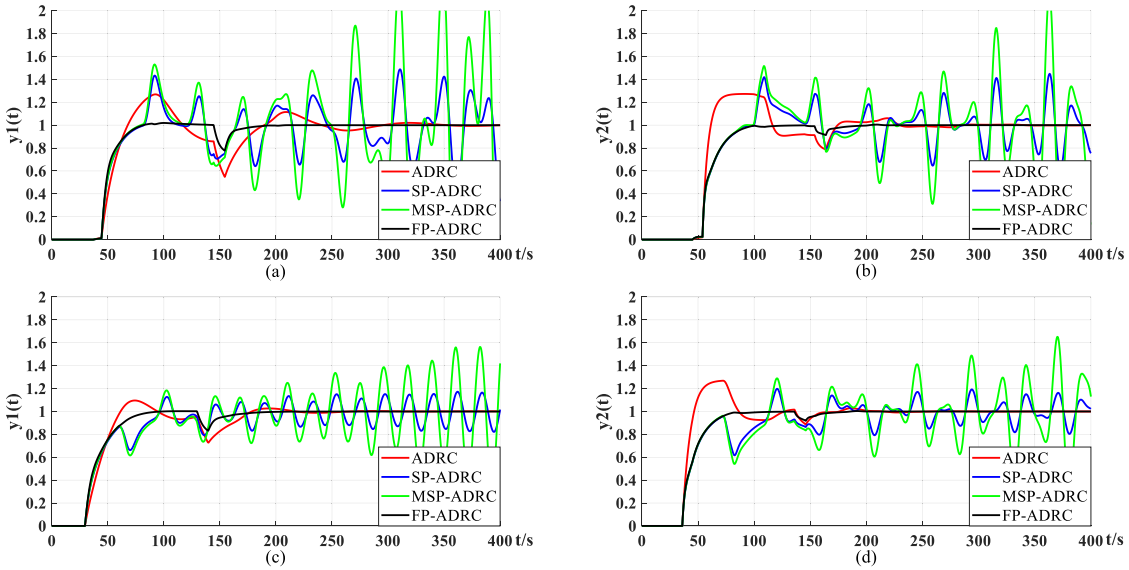

FIGURE 10. Unit step response under parameter perturbation.

of the controlled object are compared and analyzed below. The control effects when the time constant and time delay experience parameter perturbation while keeping the control parameters of the controlled object unchanged are shown in Figure 10.

As shown in Figure 10, (a) and (b) represent the temperature control response and pressure control response, respectively, when the time constant is reduced by 20% and the time-delay is increased by 20%. (c) and (d) represent the temperature control response and pressure control response, respectively, when the time constant is increased by 20% and the time delay is reduced by 20%.

In actual industrial production, due to uncontrollable factors such as variable environments and imprecise modeling of controlled objects, it is easy to have errors in modeling the controlled objects. When the parameters of the controlled object undergo perturbations, the control effect of the traditional ADRC method remains similar to when the parameters are not perturbed, and the control effect is still poor. It cannot meet the temperature and pressure requirements of the supercritical CO_2 extraction system. When the parameters of the controlled object undergo perturbations, both the SP-ADRC method and the MSP-ADRC method rely on the Smith predictor to accurately estimate the controlled object. However, the Smith predictor cannot provide an accurate estimation of the controlled object, which greatly reduces the observing performance of the LESO. As a result, the control effect of the SP-ADRC method and the MSP-ADRC method is compromised, and their steady-state performance deteriorates, leading to significant control fluctuations. When the parameters of the controlled object undergo perturbations, the FP-ADRC method proposed in this paper exhibits a control effect similar to that when there are no parameter perturbations. It still maintains good response speed and stability.

Compared with the ideal model, the FP-ADRC method proposed in this paper has better control performance compared to other methods when facing controlled objects with parameter perturbations.

C. SYSTEM RESPONSE UNDER UNCERTAINTY INTERFERENCE

In actual production processes, water in the water tank is heated by electric heating tubes, and the circulating pump then transfers the hot water to the jacket of the extraction kettle. Due to external temperature influences, there will be some heat loss in the circulation circuit. Similarly, by using a booster pump to pressurize the extraction kettle, there will be some pressure loss in the transmission path from the booster pump to the extraction kettle. To simulate these uncertainties and model mismatch problems, multiplicative output uncertainty A and B are introduced into the system. The control block diagram with uncertain disturbances is shown in Figure 11.

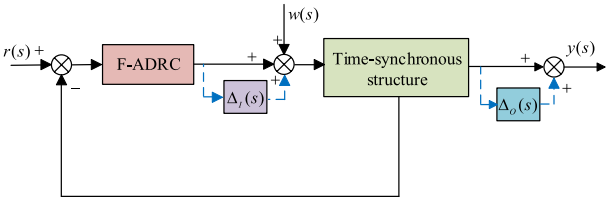

FIGURE 11. Control structure diagram with uncertain interference.

In Figure 11, the set values for A and B are

$$\Delta_I(s) = diag\left\{\frac{s+0.3}{2s+1} \quad \frac{s+0.3}{2s+1}\right\} \tag{37}$$

$$\Delta_o(s) = diag\left\{\frac{-s-0.3}{s+1} \quad \frac{-s-0.3}{s+1}\right\} \tag{38}$$

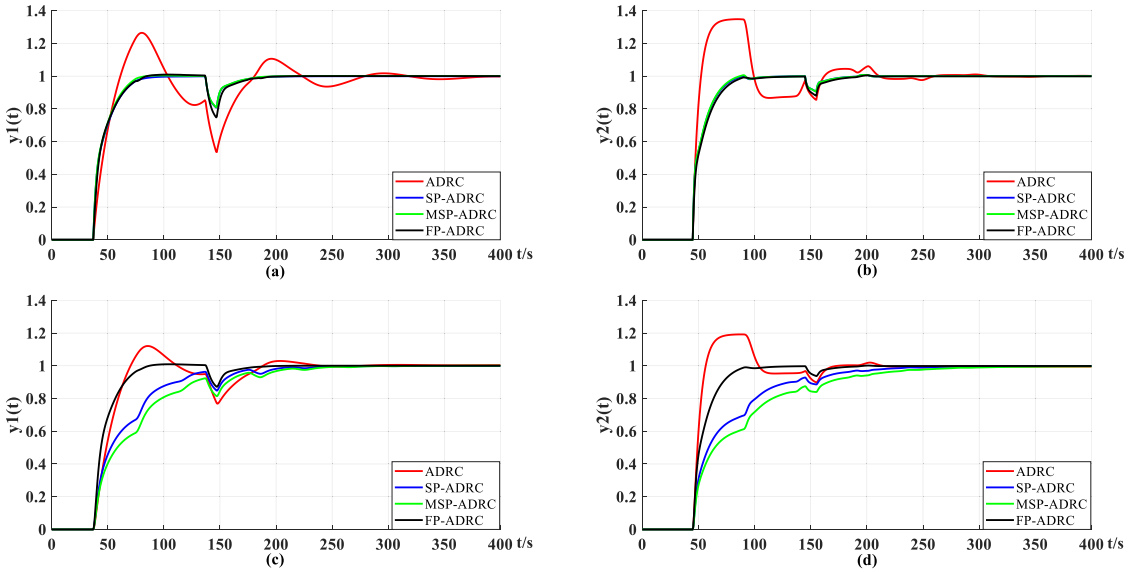

FIGURE 12. Control effect diagram after adding multiplicative uncertainty.

In equations (37) and (38), $\Delta_I(s)$ can be seen as having uncertainties of about 50% and 30% at high and low frequencies, respectively; $\Delta_o(s)$ can be seen as having errors of about 100% and 30% at high and low frequencies, respectively. The control effects of the four methods with multiplicative uncertainty are shown in Figure 12.

As shown in Figure 12, (a) and (b) represent the temperature control response and pressure control response, respectively, with multiplicative input uncertainty $\Delta_I(s)$ introduced. (c) and (d) represent the temperature control response and pressure control response, respectively, with multiplicative output uncertainty $\Delta_o(s)$ introduced.

After introducing multiplicative uncertainty, the ADRC method exhibits significant control overshoot. Due to the influence of time delay, LESO is unable to synchronously observe the dual-input signals, resulting in substantial control fluctuations and poor disturbance rejection capability.

After introducing multiplicative input uncertainty $\Delta_I(s)$, due to the accurate estimation of the controlled object by the Smith predictor, both the SP-ADRC method and the MSP-ADRC method exhibit good control performance. After introducing multiplicative output uncertainty $\Delta_o(s)$, both the SP-ADRC method and the MSP-ADRC method exhibit slow response speed and output oscillation, which cannot meet the control requirements.

The proposed FP-ADRC method in this paper improves the observation effect of LESO by proportionally reducing the lag of the output feedback through a time-synchronous structure. When multiplicative uncertainty is introduced, it can fully exploit the estimation and compensation performance of LESO, and the controller still maintains good control performance. By introducing fuzzy control principles to adaptively adjust the parameters of the error feedback control law, the static stability of the system is further enhanced.

D. EXPERIMENT VALIDATION

To verify the feasibility and effectiveness of the proposed algorithm, a temperature and pressure control experimental device was selected for experimental validation, as shown in Figure 13. The communication between Matlab, the upper computer, and the PLC was achieved through the OPC toolbox, and the proposed algorithm was applied to temperature and pressure control.

FIGURE 13. Equipment diagram for temperature-pressure control.

Set the temperature and pressure to the actual extraction requirements, which are 50°C and 32.7MPa. The temperature and pressure control curves based on the experimental platform are shown in Figures 14 and 15.

From Figures 14 and 15, it can be observed that the temperature control curve has an overshoot of approximately 2°C, while the pressure control curve has virtually no overshoot and exhibits good responsiveness. This validates the feasibility of the proposed method in practical control environments. It demonstrates good control performance in addressing the

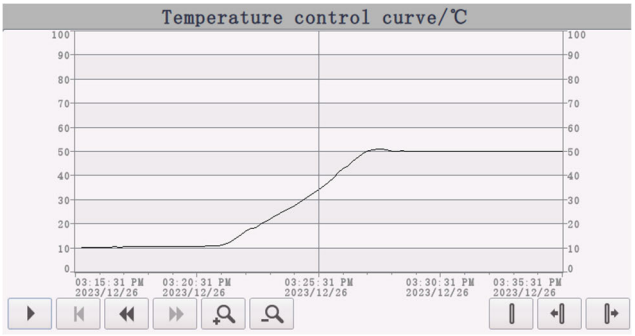

FIGURE 14. Temperature control curve.

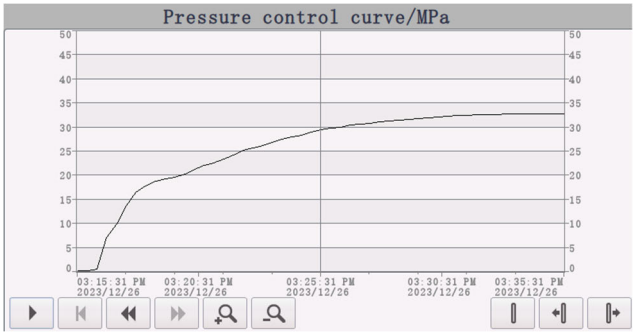

FIGURE 15. Pressure control curve.

challenging issues of strong coupling and time delay in temperature and pressure control.

VI. CONCLUSION

This paper proposes a pole-approximation-based inverse decoupling fuzzy ADRC method to address the strong coupling and time delay issues in temperature pressure control of supercritical CO_2 extraction systems, achieving stable control of temperature and pressure.

Through simulation analysis, this method has good decoupling performance, tracking performance, anti-interference ability, and robust stability. Especially in industrial production, the controlled system is subject to parameter perturbations and uncertainties due to environmental and other factors. Finally, the feasibility of this method was verified through experimental verification on a real-time platform.

In future research, we will strive to promote the practical application of this method and apply it to the control of multiple extraction reactors through development and research. By studying other methods to solve the control problem of time-delay controlled objects with coupling links, such as Back-stepping method.

The results of this study have important scientific and practical value, demonstrating good practical application prospects. This study provides a new control method and idea for temperature and pressure control, which is not limited to supercritical CO_2 extraction systems.

REFERENCES

[1] A. A. Alsaedi, M. S. Hossain, V. Balakrishnan, A. N. Ahmad Yahaya, N. Ismail, M. Naushad, C. Bathula, and M. I. Ahmad, "Extraction of municipal sewage sludge lipids using supercritical CO_2 for biodiesel production: Mathematical and kinetics modeling," *J. Chem.*, vol. 2022, pp. 1–11, Sep. 2022, doi: 10.1155/2022/7349052.

[2] A. Said, C. Guinot, J-C Ruiz, A. Grangjean, P. Dole, C. Joly, and Y. Chalamet, "Modeling of supercritical CO_2 extraction of contaminants from post-consumer polypropylene: Solubilities and diffusion coefficients in swollen polymer at varying pressure and temperature conditions," *Chem. Eng. Res. Design*, vol. 117, pp. 95–109, Oct. 2017, doi: 10.1016/j.cherd.2016.10.020.

[3] L. Yang, "Effect of temperature and pressure of supercritical CO_2 on dewatering, shrinkage and stresses of eucalyptus wood," *Appl. Sci.*, vol. 11, no. 18, p. 8730, Sep. 2021, doi: 10.3390/app11188730.

[4] W. Meng, L. Hushan, G. Youshan, and X. Hao, "Active disturbance rejection decoupling control for independent-metering electro-hydraulic system with online compensation information," *IEEE Access*, vol. 11, pp. 121539–121555, 2023, doi: 10.1109/ACCESS.2023.3328620.

[5] B. Zhang, J. Li, and W. Tan, "On model-assisted active disturbance rejection control for two-input two-output systems with time delay," *Control Theory Appl.*, vol. 38, no. 8, pp. 1229–1237, 2021, doi: 10.7641/CTA.2021.00288.

[6] P. Li, X. Yang, and Y. A. W. Shardt, "Simultaneous robust, decoupled output feedback control for multivariate industrial systems," *IEEE Access*, vol. 6, pp. 6777–6782, 2018, doi: 10.1109/ACCESS.2018.2790803.

[7] L. Shen, Z. Chen, and J. He, "Multi-zone integrated iterative-decoupling control of temperature field of large-scale vertical quenching furnaces based on ESRNN," *Processes*, vol. 11, no. 7, p. 2106, Jul. 2023, doi: 10.3390/pr11072106.

[8] J. B. Liu, W. Sun, X. Zhang, X. Ma, and T. Zou, "A feed forward decoupling strategy based on control model for the engineering application of multi-variable predictive control," *Control Decis.*, vol. 34, no. 5, pp. 1094–1102, 2019, doi: 10.13195/j.kzyjc.2017.1371.

[9] J. Wu, M. Mo, J. Li, Y. Zhang, X. Zhang, and X. Fan, "Inverse decoupling internal model control for multilevel buck converter with constant power load," *Energy Rep.*, vol. 9, pp. 1181–1189, Sep. 2023, doi: 10.1016/j.egyr.2023.04.109.

[10] Y. Hou, H. Zou, and J. Bai, "An improved anti-interference predictive PI for first order plus dead time processes," *Can. J. Chem. Eng.*, vol. 102, no. 1, pp. 324–332, Jan. 2024, doi: 10.1002/cjce.25033.

[11] A. Makhbouche, B. Boudjehem, I. Birs, and C. I. Muresan, "Fractional-order PID controller based on immune feedback mechanism for time-delay systems," *Fractal Fractional*, vol. 7, no. 1, p. 53, Jan. 2023, doi: 10.3390/fractalfract7010053.

[12] H. Zhang and T. Wang, "Finite-time sliding mode control for uncertain neutral systems with time delays," *IEEE Access*, vol. 9, pp. 140446–140455, 2021, doi: 10.1109/ACCESS.2021.3119628.

[13] J. Han and W. Zhang, "Active disturbance rejection control for large time delay systems," *Control Decis. Making*, vol. 4, pp. 67–71, Jul. 1999.

[14] J. Han, "Active disturbance rejection controller and its application," *Control Decis. Making*, vol. 13, no. 1, pp. 19–23, Jan. 1998.

[15] Z. Gao, "On the foundation of active disturbance rejection control," *Control Theory Appl.*, vol. 30, no. 12, pp. 1498–1510, 2013, doi: 10.7641/CTA.2013.31087.

[16] Z. Gao, "ADRC: The deep roots and the latest developments," *Control Theory Appl.*, vol. 40, no. 3, pp. 593–595, 2023, doi: 10.7641/CTA.2023.21112.

[17] H. Jin and Z. Gao, "On the notions of normality, locality, and operational stability in ADRC," *Control Theory Technol.*, vol. 21, no. 1, pp. 97–109, Feb. 2023, doi: 10.1007/s11768-023-00131-4.

[18] Q. Zheng and Z. Gao, "Predictive active disturbance rejection control for processes with time delay," *ISA Trans.*, vol. 53, no. 4, pp. 873–881, Jul. 2014, doi: 10.1016/j.isatra.2013.09.021.

[19] D. Zhang, X. Yao, Q. Wu, and Z. Song, "ADRC based control for a class of input time delay systems," *J. Syst. Eng. Electron.*, vol. 28, no. 6, pp. 1210–1220, Dec. 2017, doi: 10.21629/JSEE.2017.06.19.

[20] T. Zhao, Y. Cheng, L. Hua, H. Li, and Z. Chen, "Tuning of active disturbance rejection control for time-delay systems via quantitative feedback theory," *Control Theory Appl.*, vol. 38, no. 5, pp. 578–586, 2021, doi: 10.7641/CTA.2020.00494.

[21] S. N. F. Nahri, S. Du, and B. J. van Wyk, "Predictive extended state observer-based active disturbance rejection control for systems with time delay," *Machines*, vol. 11, no. 2, p. 144, Jan. 2023, doi: 10.3390/machines11020144.
[22] Y. Bai, J. Yao, and J. Hu, "A new state observer for active disturbance rejection control with measurement noise and output delay using the PDE-back stepping predictor," *ISA Trans.*, vol. 142, pp. 562–572, Nov. 2023, doi: 10.1016/j.isatra.2023.07.013.
[23] E. J. Klein, G. Johann, E. A. D. Silva, and M. G. A. Vieira, "Mathematical modeling of supercritical CO_2 extraction of *Eugenia pyriformis* Cambess. leaves," *Chem. Eng. Commun.*, vol. 208, no. 11, pp. 1543–1552, Nov. 2021, doi: 10.1080/00986445.2020.1798936.
[24] B. Li and W. You, "Solubility optimal system for supercritical fluid extraction based on a new nonlinear temperature-pressure decoupling model constructed with unequal-interval grey optimal models and Peng-Robinson models," *Math. Problems Eng.*, vol. 2018, pp. 1–11, 2018, doi: 10.1155/2018/4817565.
[25] D. Li, W. Yu, and Q. Jin, "Stability region analysis of linear active disturbance rejection controllers for first order systems with time delay," *Control Theory Appl.*, vol. 34, no. 9, pp. 1244–1249, 2017, doi: 10.7641/CTA.2017.60717.
[26] X. Zhao, G. Chen, and H. Jin, "Sliding mode active disturbance rejection control for PMSM based on improved grey wolf optimization algorithm," *J. Motor Control*, vol. 26, no. 11, pp. 132–140, 2022, doi: 10.15938/j.emc.2022.11.014.
[27] Y. Wang, W. Tan, W. Cui, W. Han, and Q. Guo, "Linear active disturbance rejection control for oscillatory systems with large time-delays," *J. Franklin Inst.*, vol. 358, no. 12, pp. 6240–6260, 2021, doi: 10.1016/J.JFRANKLIN.2021.06.016.
[28] Y. Cheng, Z. Chen, M. Sun, and Q. Sun, "Multivariable inverted decoupling active disturbance rejection control and its application to a distillation column process," *Acta Automatica Sinica*, vol. 43, no. 6, pp. 1080–1088, 2017, doi: 10.16383/j.aas.2017.c170137.
[29] R. Zhou, W. Han, and W. Tan, "On applicability and tuning of linear active disturbance rejection control," *Control Theory Appl.*, vol. 35, no. 11, pp. 1654–1662, 2018, doi: 10.7641/CTA.2018.80249.
[30] X. Sun, J. Yao, and W. Deng, "Active disturbance rejection adaptive control of multi-degrees of freedom hydraulic manipulators," *Int. J. Adapt. Control Signal Process.*, vol. 36, no. 11, pp. 2880–2902, Nov. 2022, doi: 10.1002/acs.3482.

MENGLONG CAO was born in Shandong, China, in 1971. He received the Ph.D. degree in navigation guidance and control theory from Harbin Institute of Technology, Harbin, China, in 2009. He is currently a Professor with the College of Automation and Electronic Engineering, Qingdao University of Science and Technology, China. He is also a Principal Member of the Institute of Autonomous Navigation and Intelligent Control, Qingdao University of Science and Technology. He is also the Vice Dean of the College of Automation and Electronic Engineering, Qingdao University of Science and Technology. His research interests include intelligent control, autonomous navigation, and information fusion.

ZHAOSEN ZHU was born in Shandong, China, in 1997. He is currently pursuing the master's degree in control science and engineering with Qingdao University of Science and Technology, Shandong. His main research interest includes intelligent control.

YUNPENG JU received the M.S. degree in control theory and control engineering and the Ph.D. degree in mechanical design and theory from Qingdao University of Science and Technology, in 2013 and 2016, respectively. He is currently a Master's Supervisor. His research interests include mechanical dynamics, robot control and navigation, and modeling and control of complex nonlinear systems.